Research Square

Preprints are preliminary reports that have not undergone peer review.
They should not be considered conclusive, used to inform clinical practice,
or referenced by the media as validated information.

Physical-Hydraulic Characterization of a Tropical Oxisol Profile: Implications for Urban Cemetery Suitability

Édipo Rafael dos Santos
Universidade Estadual de Ponta Grossa
José Valdirino Gaspareto
240304400000@uepg.br

Universidade Estadual de Ponta Grossa
Luiz Fernando Pires
Universidade Estadual de Ponta Grossa

Research Article

Keywords: Urban cemeteries, Brazilian Red Latosol, Soil environmental quality, São Vicente de Paula Cemetery, Necrosols

Posted Date: September 8th, 2026

DOI: https://doi.org/10.21203/rs.3.rs-10816810/v1

License: This work is licensed under a Creative Commons Attribution 4.0 International License.
Read Full License

Additional Declarations: No competing interests reported.

Physical-Hydraulic Characterization of a Tropical Oxisol Profile: Implications for Urban Cemetery Suitability

Édipo Rafael dos Santos[1], José Valdirino Gaspareto[2], Luiz Fernando Pires[3]

Affiliations

[1] Geography Graduate Program, Department of Geosciences, State University of Ponta Grossa, Av. General Carlos Cavalcanti, 4748 - Uvaranas, Ponta Grossa, 84030-900, Paraná, Brazil.

[2] Physics Graduate Program, Department of Physics, State University of Ponta Grossa, Av. General Carlos Cavalcanti, 4748 - Uvaranas, Ponta Grossa, 84030-900, Paraná, Brazil.

[3] Department of Physics, State University of Ponta Grossa, Av. General Carlos Cavalcanti, 4748 - Uvaranas, Ponta Grossa, 84030-900, Paraná, Brazil.

Corresponding author

Email address: 240304400000@uepg.br

Contributing authors: 240401000006@uepg.br; lfpires@uepg.br

List of Symbols and Acronyms

AC Soil Aeration Capacity

Fis Fissure Pores

Mac Macroporosity

Mes Mesoporosity

Mic Microporosity

n van Genuchten retention curve slope/shape parameter

PC1 First Principal Component

PC2 Second Principal Component

r^2 Coefficient of determination

Str Storage Pores

TP Total Porosity

Tr Transmission Pores

α van Genuchten air-entry parameter

θ Volumetric water content

θ_s Saturated volumetric water content

ρ_b Soil bulk density

ρ_s Particle density

CV Coefficient of Variation

L1–L10 Soil profile layers 1 through 10
PCA Principal Component Analysis
RMSE Root Mean Square Error

Abstract

Physical and hydraulic properties of urban soils strongly influence gas exchange and liquid movement; however, high-resolution physical data for undisturbed tropical soils in burial environments remain scarce. This study evaluated the vertical variation of physical properties and water retention dynamics in a 2.0-m Oxisol profile located at the São Vicente de Paula cemetery in Ponta Grossa, Southern Brazil. Undisturbed soil cores were collected across ten depth layers (0.2 m intervals) to determine bulk density, pore size distribution, and soil water retention curves fitted with the van Genuchten model. Microporosity dominated the entire profile (~67% of total porosity), maintaining high physical water storage capacity throughout depth. Soil bulk density peaked in the surface (0–0.2 m) and deep (>1.6 m) layers, whereas total porosity, macroporosity, and aeration capacity were highest in intermediate layers (0.4–1.2 m). Consequently, structural drainage and air-filled porosity decreased in deeper layers. While intermediate layers exhibit structural traits favorable for soil aeration, the high microporosity and water retention at depth indicate physical constraints on vertical fluid flux. As a single-profile baseline characterization, these physical-hydraulic parameters provide preliminary baseline data on soil physical structure, though further spatial replication and direct contaminant transport studies are required to assess environmental risk.

Keywords: Urban cemeteries; Brazilian Red Latosol; Soil environmental quality; São Vicente de Paula Cemetery; Necrosols.

Highlights

- Soil profile functionality was controlled by pore-size distribution.
- Intermediate layers favored aeration, drainage, and microbial activity.
- Deeper layers acted as water and solute retention zones.
- PCA confirmed the functional differentiation along the soil profile.
- The Oxisol displayed characteristics favorable for cemetery use.

Introduction

The consolidation of cemeteries as formal spaces designated for burial, especially after their relocation away from urban centers for sanitary reasons, did not

eliminate the geoenvironmental risks associated with human decomposition, but rather redefined them within expanding urban landscapes (Jenner 2005). As cities expand and encompass these burial sites, the environmental impacts of cemetery operations have drawn increasing scrutiny from public health authorities and urban planners (Lins et al. 2019). In Brazil, environmental regulations recognize the potential of cemeteries to pollute surrounding soil and groundwater resources (Baum et al. 2021; Morandi et al. 2024). However, many historical cemeteries operate without adequate geoenvironmental characterization or engineered barrier systems.

During organic decomposition, the primary environmental concern is the generation of necroleachate, a complex liquid effluent with high biochemical oxygen demand, elevated concentrations of dissolved organic carbon, inorganic salts, heavy metals, and potential pathogenic microorganisms (Żychowski and Bryndal 2015; Neckel et al. 2017; Mordhorst et al. 2022; Tewari et al. 2025). In cemeteries where burials occur directly in unlined soil, the physical and hydraulic properties of the unsaturated vadose zone serves as the primary natural medium governing both oxygen transport, essential for aerobic soft-tissue breakdown, and liquid percolation toward underlying aquifers (Junkins and Carter 2017; Marini et al. 2025).

Many tropical urban cemeteries in Brazil are established on highly weathered Red Latosols (Oxisols) (Schaefer et al. 2025). These soils characteristically feature a strongly aggregated, granular structure that yields high total porosity, yet they are dominated by low-activity clays that promote intense internal microporosity (Ottoni et al. 2025). Despite their widespread distribution, a major scientific gap remains: environmental impact assessments and urban planning frameworks in tropical cemeteries frequently rely on basic textural classifications or hydrological models developed for temperate soils. These simple metrics fail to quantify how the dual structural nature of Oxisols, balancing high physical water retention with rapid macro-pore drainage, varies continuously across the upper two meters of the soil profile where burials take place.

To address this gap, this study presents a single-profile baseline characterization of the physical and hydraulic properties of an Oxisol profile (0–2.0 m depth) located at the São Vicente de Paula Cemetery in Ponta Grossa, Southern Brazil. Rather than evaluating active contaminant transport directly, our primary objective is to quantify the intrinsic physical constraints governing fluid and gas dynamics across depth.

Specifically, we address two key research questions: 1) How do structural bulk density and functional pore-size distribution (micro-, meso-, and macroporosity) shift vertically across the burial horizon (0–2.0 m)? and 2) Does the soil matrix exhibit

sufficient aeration capacity in intermediate layers to support gas exchange while maintaining physical water retention in deeper layers?

We hypothesize that structural aggregation in intermediate soil layers creates high macro/mesoporosity favorable for soil aeration, whereas dominant microporosity in deeper layers provides high physical water retention that acts as a structural retardant to rapid vertical water flux. By establishing these baseline physical-hydraulic parameters, this work provides fundamental physical boundary data necessary for future spatial evaluations, numerical transport modeling, and sustainable land-use planning in tropical urban ecosystems.

Materials and Methods

Study area and baseline sampling strategy

Soil sampling was conducted in the municipality of Ponta Grossa, Paraná State, Southern Brazil, immediately adjacent (~30 m) to the active burial area of the São Vicente de Paula Cemetery (UTM 22S 588322.01E, 7223368.99N; Figure 1). The climate is classified as Cfb (subtropical highland) under the Köppen system, with well-distributed annual rainfall between 1,400 and 1,800 mm and no dry season (da Cruz 2020). The local lithology comprises Devonian siltstones and mudstones of the Paraná Basin (Grahn et al. 2010). The soil is classified as a deep, highly weathered Rhodic Hapludox (Oxisol / *Latosolo Vermelho*) according to USDA Soil Taxonomy (Soil Survey Staff 2014).

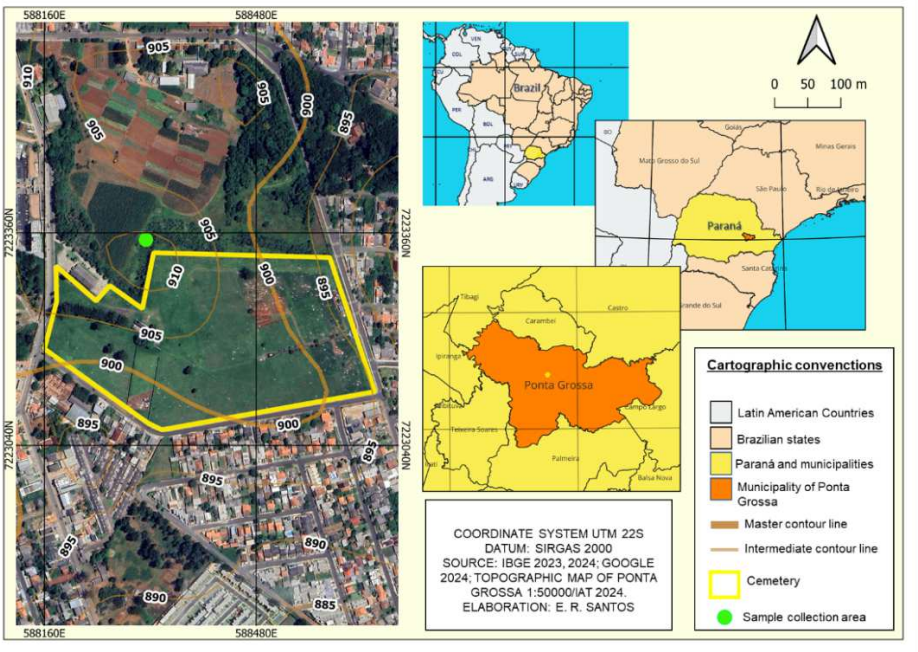


Fig. 1. Geographic location map of the study area, highlighting the regional setting, local administrative boundaries, the urban cemetery site, and the diagnostic soil profile sampling trench.

Due to regulatory restrictions and the high density of existing graves within the cemetery grounds, excavating a large deep trench inside the active burial section was unfeasible without destroying existing grave architecture. Consequently, sampling was established in an undisturbed native soil area directly adjacent to the burial plots. This sampling location belongs to the exact same soil mapping unit, parent material, and topographic position (upper slope) as the cemetery. This strategy was intentionally chosen to characterize the unmanaged, baseline physical-hydraulic properties of the native Oxisol matrix, providing diagnostic boundary conditions free from severe anthropogenic physical turning or structural backfilling.

In July 2024, a single representative trench (3.0 m long × 3.0 m × 2.0 m deep) was excavated. Soil samples were collected across ten depth layers at 0.20 m regular intervals (designated L1 through L10, covering 0.10 m to 1.90 m depth), spanning both the shallow surface soil and the subsoil beneath the typical regional burial depth (~1.0 m) (Figure 2). Disturbed samples were collected for particle-size distribution. Undisturbed soil cores (5.0 cm height × 5.0 cm diameter; V ≈ 98.2 cm^3) were sampled in replicate (n = 8 cores per layer; 80 undisturbed cores total) using steel volumetric rings carefully driven into the soil at field water capacity to minimize structural deformation (Teixeira et al. 2017).



Fig. 2. Representative field photograph of the São Vicente de Paula Cemetery grounds, illustrating intensive hand-excavation of burial pits, high grave density, and exposed reddish Oxisol profile material across the landscape.

Particle-size analysis

Soil textural fractions (sand, silt, and clay) were determined following Donagemma et al. (2017). Air-dried fine earth (ADFE, < 2 mm) samples (20 g) were chemically dispersed in 1 mol L^{-1} NaOH and distilled water, soaked for 12 h, and subjected to ultrasonic agitation (5 min, 20% amplitude in an ice bath). The sand

fraction (> 53 µm) was separated by wet sieving and dried at 40 °C for 48 h. The clay fraction (< 2 µm) was quantified using the pipette method based on Stokes' Law sedimentation velocity (Zhang 2023), adjusting for chemical dispersant mass. Silt was determined by mass balance. Particle size distribution across the 10 layers is presented in Table 1.

Table 1. Particle-size distribution (sand, silt, clay %) across depth layers (L1 to L10) of the studied Oxisol profile (mean ± standard deviation, n = 3).

Layer	Depth Range (m)	Sand (%)	Silt (%)	Clay (%)	Textural Class
L1	0.00–0.20	6.82±0.12	51.38±3.83	41.80±3.73	Silty Clay
L2	0.20–0.40	4.79±0.22	51.57±8.21	43.63±8.40	Silty Clay
L3	0.40–0.60	4.64±0.13	37.36±3.62	58.00±3.75	Clay
L4	0.60–0.80	4.66±0.40	37.36±2.08	73.70±2.46	Clay
L5	0.80–1.00	4.30±0.20	37.36±2.59	68.60±2.55	Clay
L6	1.00–1.20	4.40±0.25	37.36±0.44	70.87±0.57	Clay
L7	1.20–1.40	4.28±0.34	37.36±2.53	73.37±2.73	Clay
L8	1.40–1.60	4.19±0.27	18.67±0.25	77.13±0.50	Clay
L9	1.60–1.80	4.88±0.13	24.82±2.46	70.30±2.59	Clay
L10	1.80–2.00	4.53±0.18	22.32±1.01	73.13±1.19	Clay

Bulk density and total porosity

Soil bulk density (ρ_s, g cm^{-3}) was determined via the oven-dry mass method (105°C for 48 h) relative to the exact core cylinder volume (≈98.2 cm^3) (Blake and Hartge 1986). Total porosity (TP, cm^3 cm^{-3}) was calculated directly from volumetric soil water content at complete saturation (θ_s), assumed equivalent to total pore volume prior to tension drainage (Teixeira et al. 2017).

Pore size classes and aeration capacity

Pore size distributions were categorized according to equivalent pore diameter (d, µm) calculated via the Young-Laplace capillary equation (d = 3000/h, where h is pressure head in cm H_2O): 1) Macropores (Mac, d > 100 µm), drained between saturation (θ_s) and a tension head of 30 cm H_2O (Kong et al. 2021); 2) Mesopores (Mes, 30 ≤ d ≤ 100 µm), drained between pressure heads of 30 and 100 cm H_2O (Kong et al. 2021); 3) Micropores (Mic, d < 30 µm), water retained at a pressure head of 100 cm H_2O; and 4) Aeration Capacity (AC): Calculated as $AC = \theta_s - \theta_{FC}$, where field capacity ($\theta_{FC}$) corresponds to soil water retention at 100 cm H_2O (Hegde et al. 2026).

Functional pore size classification

To complement physical diameter classes, functional pore categories were assigned following Greenland's (1977) functional pore framework: 1) Fissure pores (d > 500 μm), associated with rapid crack drainage and macro-aeration (h > 6 cm H_2O); 2) Transmission pores (50 ≤ d ≤ 500 μm), facilitating main gravitational drainage and root growth (60 cm H_2O ≤ d ≤ 6 cm H_2O); and 3) Storage pores (d < 50 μm), retaining plant- and microbe-available water against gravity (h < 60 cm H_2O).

Water retention curves and van Genuchten modeling

Undisturbed cores (n = 8 per layer) were saturated gradually by capillary wetting from the base (0.5 cm h^{-1}) for 24 h. Saturated cores were transferred to tension tables and subjected to sequential pressure heads ranging from 10 to 100 cm H_2O at 10 cm H_2O intervals. Hydraulic equilibrium at each suction step was confirmed by cessation of water outflow from drainage tubes before core mass determination. Soil dry mass (105°C) was subsequently recorded to calculate volumetric water content (θ) at each pressure head (Teixeira et al. 2017; Fu et al. 2021).

Partial soil water retention curves (SWRC) over the 0 to 100 cm H_2O range were fitted using the van Genuchten (1980) non-linear model:

$$\theta(h) = \theta_r - \frac{\theta_s - \theta_r}{[1 + (\alpha h)^n]^m}$$

where θ(h) is volumetric water content (cm^3 cm^{-3}) at pressure head h (cm H_2O), θ_r is residual water content, θ_s is saturated water content, α is an empirical parameter inversely related to air-entry pressure (cm^{-1}), and n and m (m = 1 - 1/n) are curve-shape parameters.

Parameter optimization was conducted using non-linear least-squares fitting in RETC software. High coefficients of determination (r^2 = 0.99) and minimal root mean square errors (RMSE ≤ 0.007) reflect model optimization across the controlled low-pressure head range (0 to 100 cm H_2O) measured under standardized laboratory equilibrium conditions (Table 2).

Table 2. Fitted van Genuchten (VG) model parameters across soil depth layers (L1–L10) of the studied Oxisol profile (θ_s: saturated water content; θ_r: residual water content; α: air-entry parameter; n, m: shape parameters; r^2: coefficient of determination; RMSE: root mean square error).

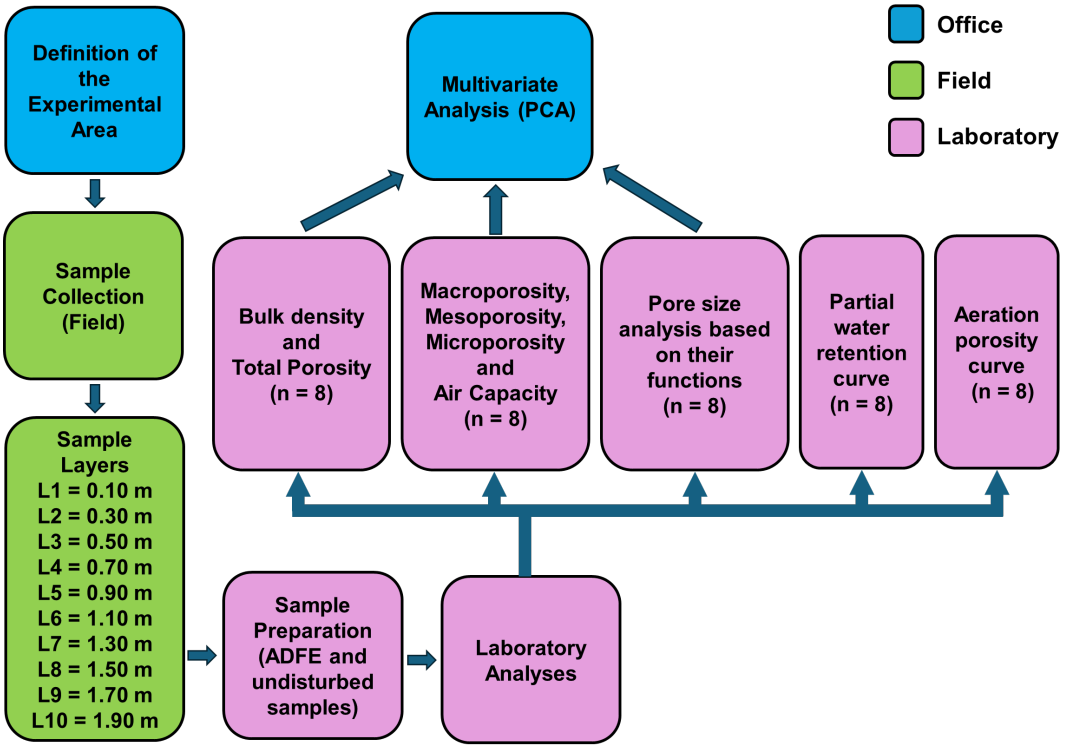
VG Model	**Soil layers**									
Parameters	**L1**	**L2**	**L3**	**L4**	**L5**	**L6**	**L7**	**L8**	**L9**	**L10**

θ_s (cm^3 cm^{-3})	0.50	0.55	0.54	0.52	0.53	0.50	0.51	0.50	0.49	0.48
θ_r (cm^3 cm^{-3})	0.28	0.13	0.19	0.20	0.24	0.24	0.14	0.01	0.00	0.00
α (cm H_2O)	0.10	0.06	0.06	0.07	0.07	0.08	0.12	0.13	0.14	0.19
n (-)	1.34	1.31	1.53	1.51	1.60	1.43	1.24	1.17	1.12	1.11
m (-)	0.25	0.24	0.35	0.34	0.37	0.30	0.19	0.14	0.11	0.10
r^2 (-)	0.99	0.99	0.99	0.99	0.99	0.99	0.99	0.99	0.99	0.99
RMSE	0.004	0.007	0.007	0.004	0.004	0.003	0.003	0.004	0.004	0.003

Statistical analysis

To assess variations in soil physical and hydraulic parameters across the vertical profile (layers L1 through L10), data were evaluated using descriptive statistics, including arithmetic means and standard deviations as metrics of central tendency and dispersion, respectively.

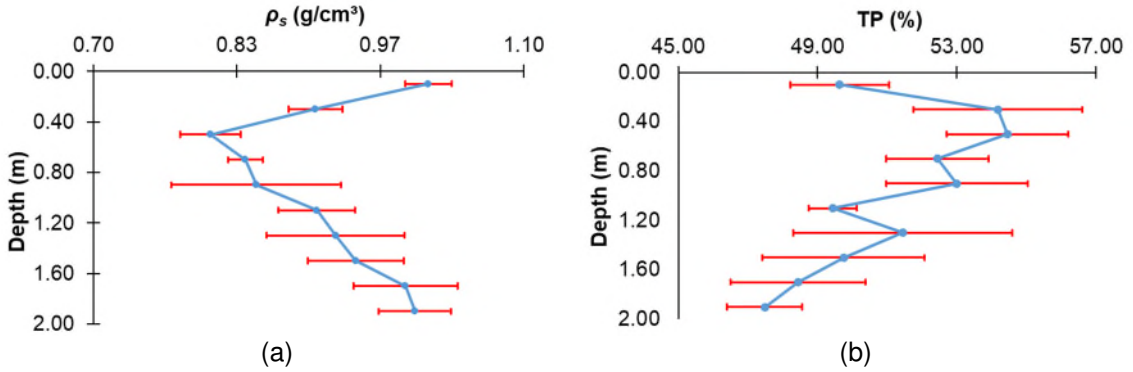
To explore complex multivariate structures and interrelationships among the physical-hydraulic attributes across soil depths, Principal Component Analysis (PCA) was performed. Prior to multivariate ordination, the dataset was autoscaled (z-score transformation) to standardize variances across variables measured in different units. PCA reduced data dimensionality into uncorrelated principal components, enabling the identification of dominant variance patterns, depth-wise sample clustering (score analysis), and parameter covariance structures (loading analysis). All descriptive statistical computations and multivariate ordinations were conducted using PAST software v4.03 (Hammer et al. 2001). A summary of the analytical workflow is presented in Figure 3.



239 Fig. 3. Methodological workflow illustrating the sequential analytical phases, including field core
240 sampling (0.0–2.0 m depth, L1–L10), sample preparation (ADFE), laboratory physical-hydraulic
241 determinations, water retention curve analysis, and multivariate statistical modeling (PCA).
242 ADFE = air-dried fine earth (< 2 mm).
243
244 **Results**
245 **Bulk density and total porosity dynamics**

246 Soil bulk density and total porosity exhibited inverse vertical trends across the
247 2.0 m Oxisol profile (Figure 4). The highest mean ρ_s occurred in the surface layer L1
248 (1.01 g cm^{-3}), followed by a sharp drop in layer L3 (0.81 g cm^{-3}). Below L3, ρ_s increased
249 progressively with depth, reaching 1.00 g cm^{-3} in the deepest layer (L10) (Figure 4a).
250 Profile-wide, mean ρ_s was 0.92 g cm^{-3}.

251 Conversely, total porosity peaked in the upper-intermediate layers (L2–L5),
252 expanding from 49.6% in L1 to a maximum of 54.5% in L3 (Figure 4b). Beyond L5, TP
253 systematically decreased toward the base of the profile, reaching its minimum in L10
254 (47.5%). The mean TP across the profile was 51%, with spatial dispersion peaking in
255 layer L7 (CV = 6.1%).



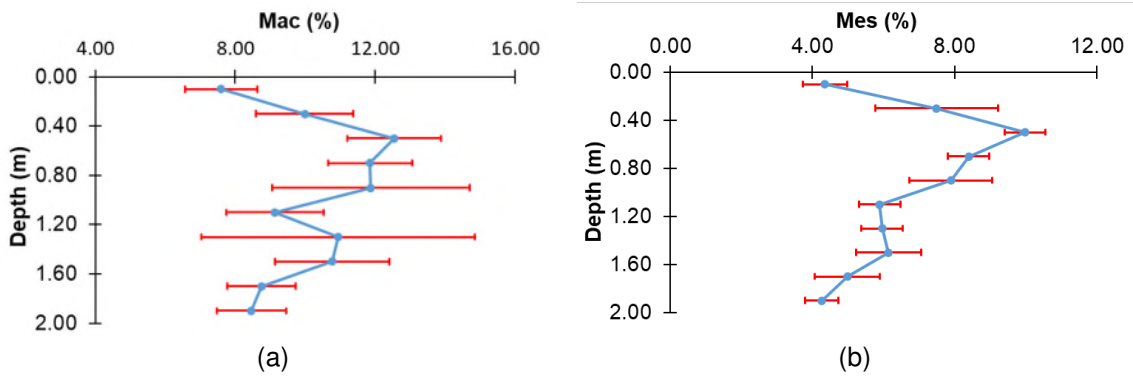
256 Fig. 4. Depth profiles (0.0–2.0 m, layers L1–L10) of (a) soil bulk density (ρ_s) and (b) total
257 porosity (TP). Points represent layer mean values, and horizontal error bars denote standard
258 deviations (n = 8 undisturbed cores per layer).

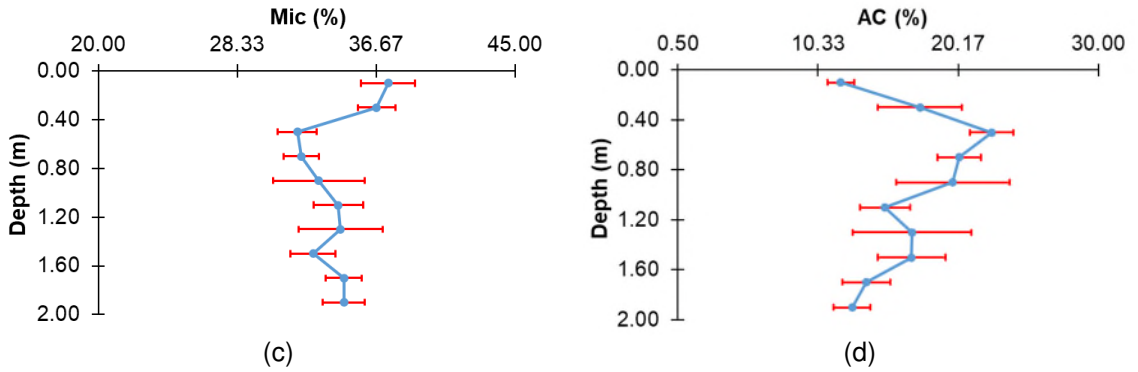
259

260 **Pore size distribution and aeration capacity**

261 Microporosity dominated the pore system throughout the profile, averaging
262 34±2% across all layers and accounting for approximately 67% of total pore volume.
263 Micropore fraction was greatest in the upper layers L1 (37.4%) and L2 (36.7%),
264 stabilizing at moderate levels (32.2% to 34.7%) from L4 down to L10 (Figure 5a).

265 Mesoporosity and macroporosity displayed parallel depth-dependent
266 trajectories (Figures 5b, 5c). Both pore classes increased from the surface to peak in
267 layer L3 (Mes = 10.0%; Mac = 12.5%), coinciding with the lowest ρ_s. Below L3, meso-
268 and macroporosity declined continuously toward deep layers, reaching profile minima
269 in layers L9–L10 (Mac < 8.8%; Mes ≈ 4.3%). Profile averages were 7±2% for
270 mesopores (13% of TP) and 10±2% for macropores (20% of TP).





271 Fig. 5. Depth profiles (0.0–2.0 m, layers L1–L10) of (a) macroporosity (Mac); (b) mesoporosity
272 (Mes); (c) microporosity (Mic); (d) aeration capacity (AC). Points represent layer mean values,
273 and horizontal error bars denote standard deviations (n = 8 undisturbed cores per layer).

274

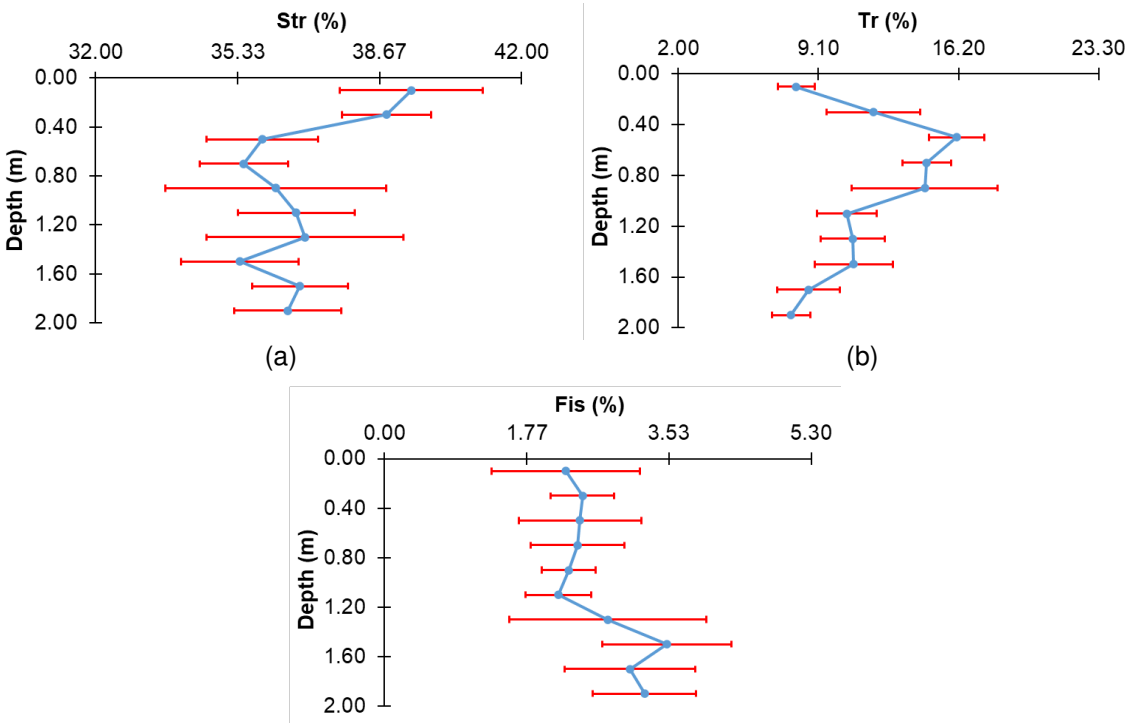
275 Soil aeration capacity was strongly governed by larger pore fractions (Mac +
276 Mes). Air-filled pore volume rose significantly from L1 (11.9%) to a maximum in L3
277 (22.5%), reflecting enhanced macro-aggregation (Figure 5d). Below L3, AC steadily
278 contracted, falling below 14% in layers L9 and L10. Overall mean AC was 17±3%, with
279 intermediate layers exhibiting higher standard deviations due to localized structural
280 heterogeneity.

281

282 **Functional pore size classes**

283 Categorization by pore functionality confirmed the structural predominance of
284 water storage over rapid transmission (Figure 6). Storage pores constituted the
285 dominant functional class across all depths, averaging 37±1% (CV ≈ 4%). Storage pore
286 volume was highest in L1–L2 (≈39%) and remained consistently elevated (35.5% to
287 36.5%) throughout intermediate and deep layers (Figure 6a).

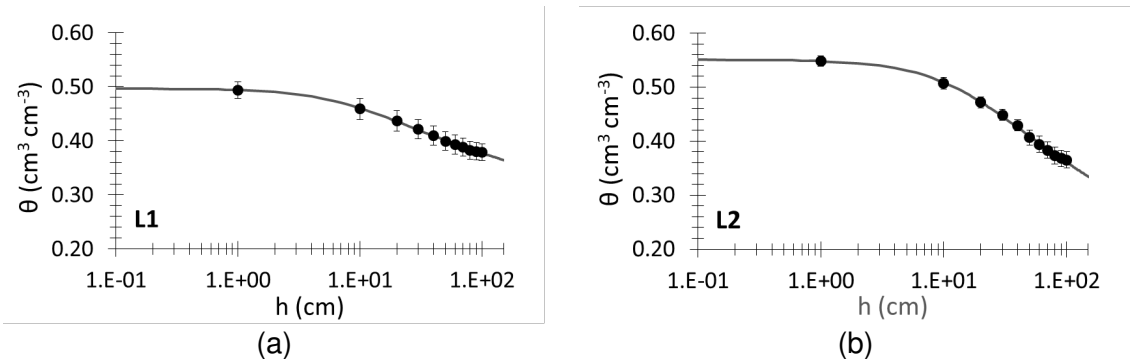
288 Transmission pores mirrored macropore trends: starting at 8.0% in L1,
289 expanding to a maximum of 16.1% in L3, and progressively declining through deep
290 layers to 7.7% in L10 (Figure 6b). Fissure pores represented the minor fraction (< 4%
291 overall, mean 2.7±0.5%). Fissures remained stable in upper and intermediate layers
292 (2.2–2.3%) but showed a minor upward trend in deep layers, peaking at 3.5% in L8 and
293 3.2% in L10 (Figure 6c).

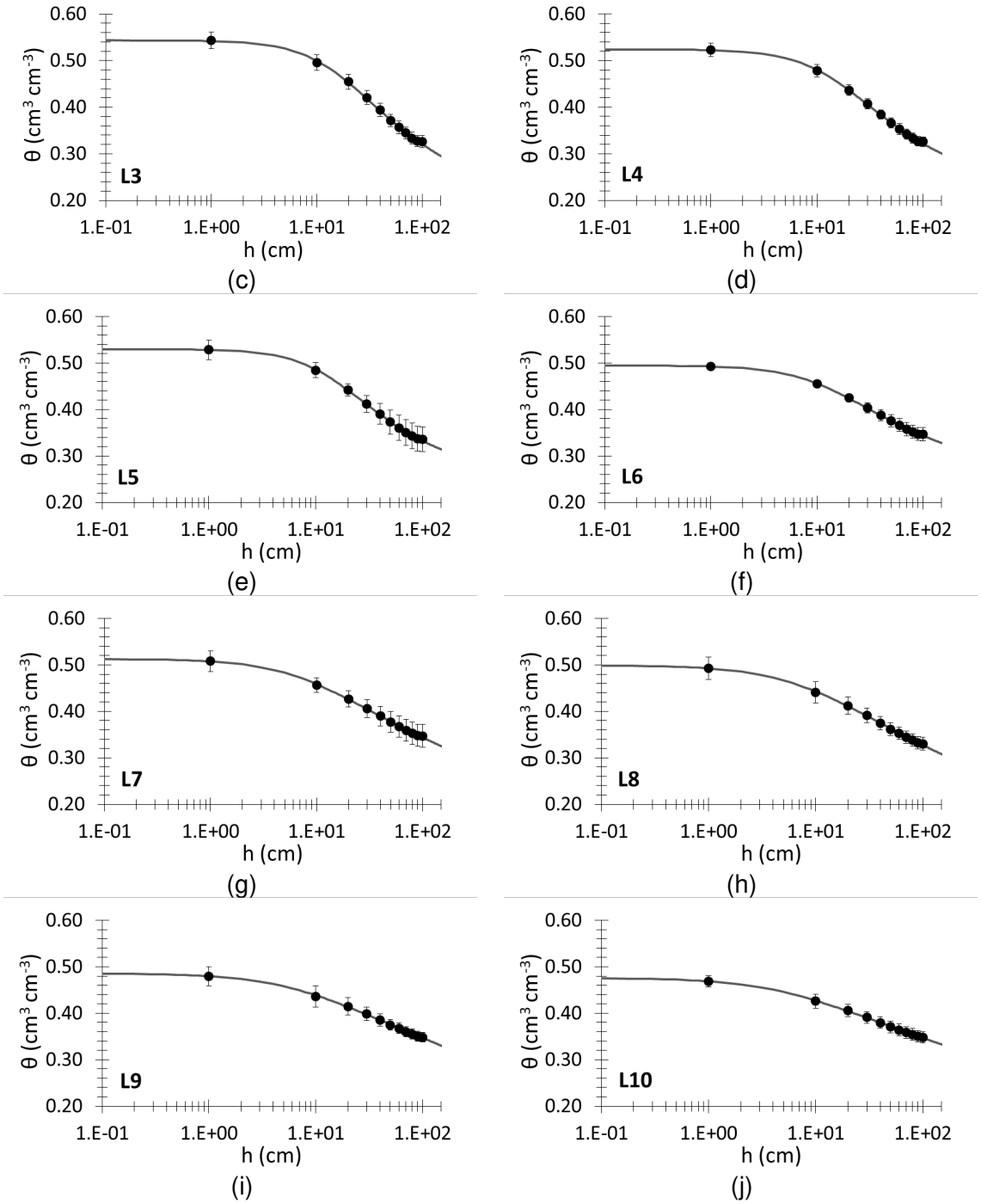


294 Fig. 6. Depth profiles (0.0–2.0 m, layers L1–L10) of (a) storage pores (Str); (b) transmission
295 pores (Tr); (c) fissures (Fis). Points represent layer mean values, and horizontal error bars
296 denote standard deviations (n = 8 undisturbed cores per layer).
297

298 **Water retention characteristics**

299 The van Genuchten model provided excellent fits to the measured partial water
300 retention data across all layers (r^2 = 0.99; RMSE ≤ 0.007; Table 2, Figure 7). Saturated
301 volumetric water content ranged from 0.476 cm^3 cm^{-3} (L10) to 0.551 cm^3 cm^{-3} (L2),
302 directly reflecting TP variations.





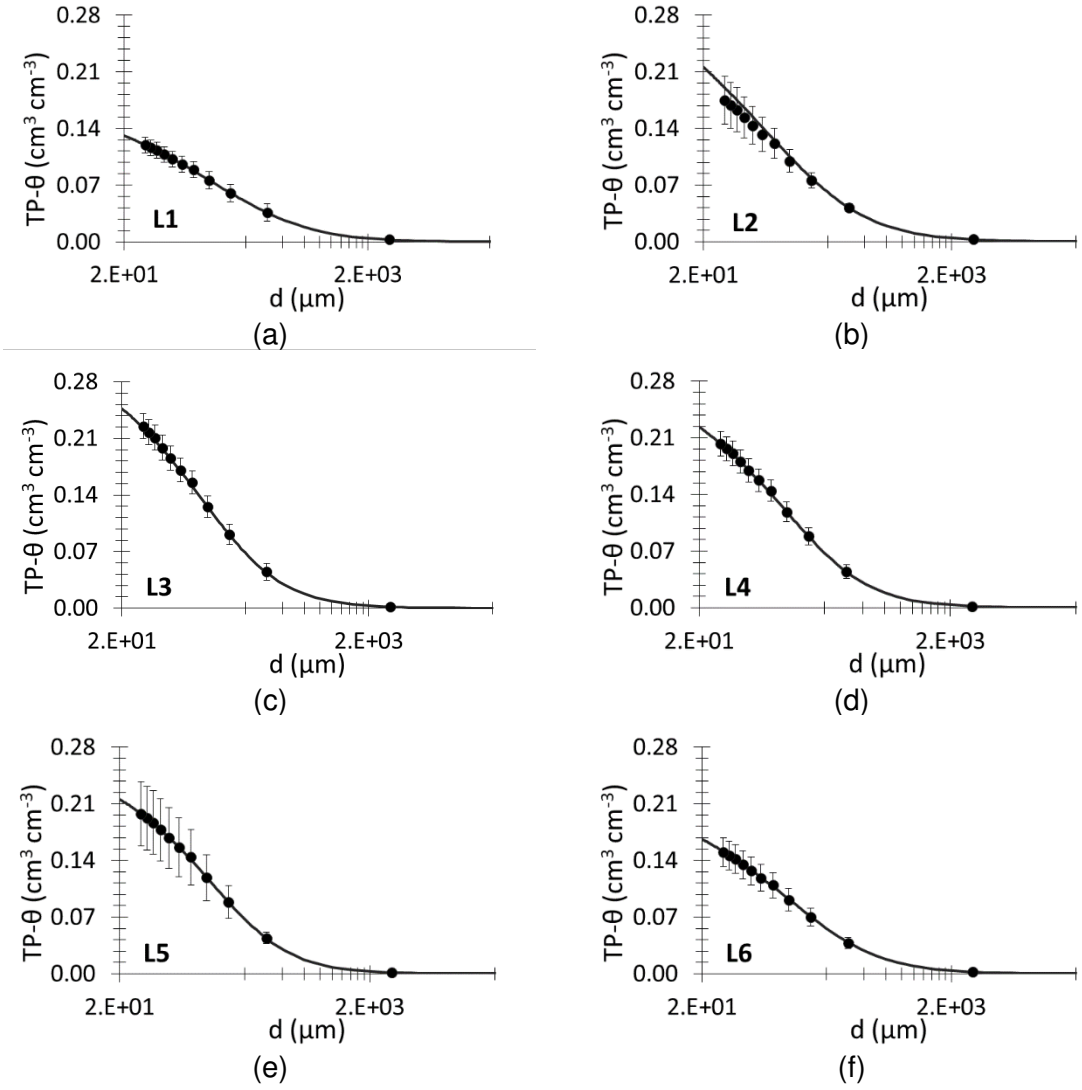
303 Fig. 7. Partial water retention curves obtained for the different layers (L1 to L10) of the Oxisol
304 studied. Volumetric water content is represented by θ and pressure head by h. Points represent
305 layer mean values, and vertical error bars denote standard deviations (n = 8 undisturbed cores
306 per layer).
307

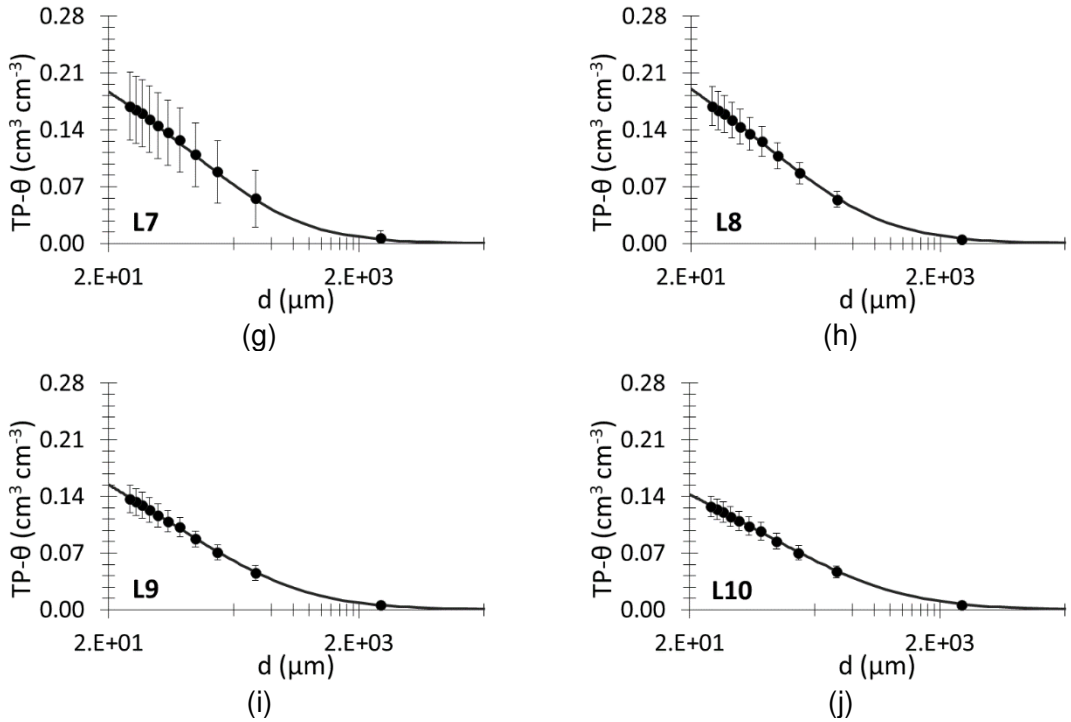
308 Tension-drainage behavior varied distinctively with depth. For example,
309 intermediate layers (L2–L6) were characterized by lower air-entry suctions (van
310 Genuchten α) and steeper retention slopes (higher n values, 1.31–1.60), indicating
311 rapid drainage of capillary water between 1 and 100 cm H_2O pressure head due to

higher macro/mesopore frequencies. On the other hand, surface (L1) and deep layers (L7–L10) displayed higher air-entry suctions (α = 0.12–0.19 cm H_2O) and flatter desorption curves (n = 1.11–1.24). The gentle slope in deep layers reflects persistent physical water retention under increasing pressure head, driven by dominant microporosity and reduced macropore availability.

Aeration porosity profiles

Aeration porosity curves (TP-θ) demonstrated progressive replacement of water by air as pore equivalent diameters decreased from > 500 µm down to 1 µm (Figure 8). Drainage was concentrated primarily within the 150 to 30 µm diameter interval (Mac and Mes equivalent range).





323 Fig. 8. Aeration porosity (TP-θ) for the different layers (L1 to L10) of the Oxisol studied. Points
324 represent layer mean values, and vertical error bars denote standard deviations (n = 8
325 undisturbed cores per layer).

326

327 Intermediate layers (L3, L4, L5) exhibited the greatest air-filled pore
328 development across all suction steps, with L3 reaching an air-filled volume of 0.244
329 $cm^3\ cm^{-3}$ at 20 µm equivalent pore diameter. Conversely, deep layers (L9 and L10) and
330 the immediate surface (L1) displayed significantly lower air-filled volumes at 20 µm
331 (0.130 to 0.152 $cm^3\ cm^{-3}$), indicating high residual water retention and lower gas-phase
332 volume following gravitational drainage.

333

334 **Multivariate ordination (PCA)**

335 Principal Component Analysis integrated the physical and functional dataset,
336 with the first two axes explaining 86.68% of total variance (PC1 = 64.18%, PC2 =
337 22.50%; Figure 9).

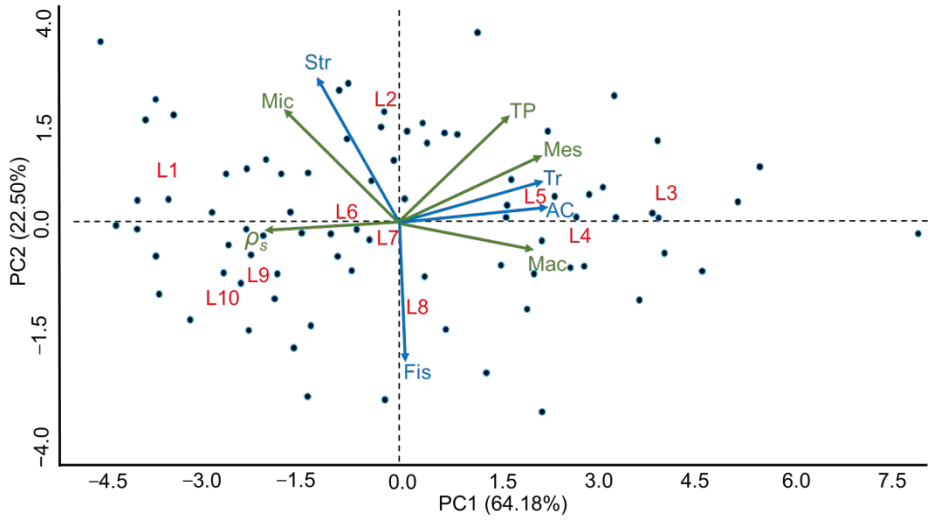


Fig. 9. Principal Component Analysis (PCA) biplot of the soil's hydrophysical and functional attributes for the studied layers (L1 to L10). Black points represent the eighty analyzed samples, while red symbols indicate the ten soil layers (L1 to L10). Green vectors depict the physical and structural properties (ρ_s: Soil bulk density; TP: Total Porosity; Mac: Macroporosity; Mes: Mesoporosity; Mic: Microporosity). Blue vectors designate the functional dynamic and water retention properties (AC: Air capacity; Tr: Transmission pores; Str: Storage pores; Fis: Fissures).

The PC1 Loadings (Structural Functionality) were positively associated with aeration capacity (0.41), transmission pores (0.40), macroporosity (0.38), and mesoporosity (0.38). Soil bulk density (-0.38) and microporosity (-0.32) loaded strongly in the negative direction (Table 3). Intermediate layers (L3, L4, L5) clustered in the positive PC1 quadrant, driven by high macroporosity and aeration. Deep layers (L6, L7, L9, L10) and surface layer L1 projected into the negative PC1 domain, aligning with high bulk density and microporosity vectors.

The PC2 Loadings (Matrix Retention vs. Fissuring) were positively influenced by storage pores (0.55), microporosity (0.41), and total porosity (0.40), separating layer L2 near the top of the axis. The fissure vector loaded strongly negative (-0.53), isolating layer L8 in the lower quadrant (Figure 9, Table 3).

Table 3 - Principal component (PC) analysis loadings for soil physical, structural, and functional properties across the studied soil profile.

Category	Variable	PC1 (64.18%)	PC2 (22.50%)
Physical and Structural Properties	ρ_s	-0.38	-0.03
	TP	0.30	0.40
	Mac	0.38	-0.10
	Mes	0.38	0.23
	Mic	-0.32	0.41
Hydraulic and Functional Properties	AC	0.41	0.05
	Str	-0.23	0.55
	Tr	0.40	0.14
	Fis	0.00	-0.53

ρ_s: Soil bulk density; TP: Total porosity; Mac: Macroporosity; Mes: Mesoporosity; Mic: Microporosity; AC: Air capacity; Str: Storage pores; Tr: Transmission pores; Fis: Fissures.

Discussion

Structural zonation and aeration dynamics in upper layers

The physical and hydraulic attributes of the evaluated Oxisol reflect a physical matrix typical of highly weathered, micro-aggregated tropical soils with low anthropogenic disturbance (de Oliveira et al. 2021). The low bulk density and high total porosity observed across the profile, particularly in intermediate layers L2–L5 (Figure 4), are linked to the characteristic gibbsitic and iron-oxide pseudo-aggregate structure of Latosols (Reatto et al. 2009). These structural conditions establish an interconnected pore network that governs both gas exchange and fluid retention across depth intervals.

In the intermediate layers (L3–L5), elevated proportions of macropores, mesopores, and transmission pores coincided with peak aeration capacity > 0.20 cm^3 cm^{-3} (Figures 5 and 6). In all layers, AC remained well above the critical biological threshold of 0.10 cm^3 cm^{-3} (Stepniewski et al. 1994), indicating that gas transport is not structurally restricted within the upper meter. The concentration of drainable pores (30–150 µm) within the burial depth zone (≈ 1 m) suggests physical pathways capable of supporting gas diffusion (Karahan and Erşahin 2017). This structural configuration provides an environment conducive to aerobic soil microbial respiration near typical burial depths (Carter et al. 2010), without displaying the continuous macropore dominance that would otherwise trigger excessive gravitational bypass flow (Ramesh et al. 2019).

Deep layer porosity and hydraulic matrix dynamics

Below layer L5, the progressive increase in bulk density (ρ_b = 1.00 g cm^{-3}) and concurrent reductions in TP, Mac, and AC demonstrate a clear transition toward a

388 micropore-dominated matrix (Figure 5a). Micropores constituted up to 67% of total pore
389 volume across the profile, with water storage pores exhibiting marked stability (CV ≈
390 4%) from L4 to L10 (Figure 6a). This pore system architecture dictates the hydraulic
391 behavior observed in the partial water retention curves (Figure 7) and aeration porosity
392 profiles (Figure 8).

393 The reduced desorption slope (lower van Genuchten n parameters) and higher
394 air-entry suctions observed in deep layers (L7–L10) indicate strong physical water
395 retention under increasing matric suction (Maia et al. 2018). While micropores promote
396 water storage and matrix stability (Pires et al. 2019; Ngolo et al. 2023), they also
397 increase tortuosity and reduce hydraulic conductivity under unsaturated conditions
398 (Hou et al. 2023). Although fissure-type pores slightly increased at depth (3.5% in L8;
399 Figure 6c), their minor relative volume (< 4%) suggests a minimal likelihood of macro-
400 fissure-driven preferential flow paths (Krzeminska et al. 2014). Consequently, while the
401 intermediate profile supports gas exchange, the deeper layers represent a physical
402 domain characterized by restricted fluid movement and elevated water retention.
403 However, whether these physical constraints translate into effective contaminant
404 attenuation requires hydrochemical and solute transport validation.
405
406 **Multivariate Integration and Study Limitations**

407 Principal Component Analysis (Figure 9) corroborated the functional vertical
408 zonation of the profile. PC1 separated the profile into two distinct functional domains:
409 an upper-intermediate domain (L3–L5) associated with high fluid transmission (Tr-
410 pores, Mac) and AC, and a deeper domain (L6–L10) defined by higher ρ_b and Mic.
411 Layer L1 occupied an isolated position along PC1, reflecting surface matrix
412 reorganization driven by environmental exposure and wetting-drying cycles (Assouline
413 2004; Orozco-López et al. 2018). PC2 highlighted matrix storage capacity in L2 and
414 local structural anomalies, such as fissure-type pores alignment in L8. Overall, the
415 multivariate analysis demonstrates that depth-dependent pore size distribution controls
416 the spatial segregation of physical functions across the profile.

417 However, some methodological constraints must be acknowledged when
418 interpreting these baseline results. Soil characterization was restricted to a single
419 diagnostic trench due to severe physical space limitations, high grave density within the
420 urban cemetery, and municipal permitting restrictions. Thus, spatial heterogeneity
421 across the broader landscape was therefore not evaluated. Sampling was conducted
422 during a single campaign, which does not capture seasonal fluctuations in soil water
423 content or transient pore network dynamic changes. Measured physical metrics provide

static physical structural boundaries; they do not quantify actual field infiltration rates, solute dispersion, or geochemical attenuation capacity.

To build upon these baseline physical findings, future research should 1) expand spatial sampling using non-invasive methods (e.g., geophysical imaging or hand augering) across surrounding urban micro-catchments; 2) perform long-term field monitoring of pressure head, seasonal water table dynamics, and in-situ hydraulic conductivity; and 3) combine physical-hydraulic characterization with hydrochemical sampling (leachate monitoring) and reactive solute transport modeling to evaluate potential contaminant mobility directly.

Conclusions

This study demonstrates that the evaluated tropical Oxisol exhibits a compartmentalized physical-hydraulic structure across depth, offering site-specific insights for urban cemetery planning. Rather than functioning as a uniform physical medium, the profile displays a distinct functional duality. The intermediate layers (L2–L5) act as a high-diffusivity aeration and fluid transmission domain capable of supporting gas exchange within typical burial depths (≈ 1 m). The deeper subsoil layers (L6–L10) transition into a capillary-dominated storage domain governed by microporosity and higher bulk density, which restricts rapid fluid movement. Furthermore, the minimal occurrence of fissure-type pores across all depths indicates that fluid and gas transport are regulated primarily by the soil's intra- and inter-aggregate matrix structure rather than preferential bypass channels.

From an urban environmental management perspective, these findings highlight the limitations of relying solely on broad textural classes or temperate soil models when evaluating cemetery suitability in tropical environments. Quantifying the vertical transition from an aerated surface/intermediate matrix to a retention-dominated subsoil provides an essential physical baseline for parameterizing local hydrogeological transport models and designing unsaturated-zone engineering barriers. Because these findings represent a diagnostic baseline from a single profile, future research incorporating multi-site spatial sampling, seasonal water content monitoring, and reactive tracer assays will be critical to fully quantify contaminant transport dynamics in cemetery tropical urban ecosystems.

Acknowledgments

The authors would like to thank the State University of Ponta Grossa (UEPG) and the administration of the São Vicente de Paula Cemetery for their support during soil sampling.

Author Contributions

Supervision and methodology, Édipo Rafael dos Santos; project administration, Luiz Fernando Pires; investigation, Édipo Rafael dos Santos and José Valdirino Gaspareto; validation, Luiz Fernando Pires; original draft preparation and major revision, Édipo Rafael dos Santos, José Valdirino Gaspareto, and Luiz Fernando Pires; review and editing, Luiz Fernando Pires; visualization and formal analysis, Édipo Rafael dos Santos. All authors have read and agreed to the published version of the manuscript.

Funding

This research was partially funded by the National Council for Scientific and Technological Development (CNPq) (Grant 303950/2023-4 and Grant 400136/2025-2) and the Coordination for the Improvement of Higher Education Personnel (CAPES) (Finance Code 001).

Data availability

Data are available from the corresponding author upon reasonable request.

Declaration of competing interest

The authors declare that they have no known competing financial interests or personal relationships that could have appeared to influence the study reported in this paper.

Use of IA

During the preparation of this work, the author(s) used Grammarly in order to make grammatical corrections. After using this tool/service, the author(s) reviewed and edited the content as needed and take full responsibility for the content of the published article.

References

Assouline S (2004) Rainfall-Induced Soil Surface Sealing: A Critical Review of Observations, Conceptual Models, and Solutions. Vadose Zone J 3:570–591. https://doi.org/10.2136/vzj2004.0570

Baum CA, Becegato VA, Lavnitcki L, et al (2021) Evaluation of soil contamination by heavy metals at public cemeteries in the municipality of Lages, southern Brazil. Eng Sanit E Ambient 26:883–891

Blake GR, Hartge KH (1986) Bulk Density. In: Klute A (ed) SSSA Book Series, 1st edn. Wiley, pp 363–375

Carter DO, Yellowlees D, Tibbett M (2010) Moisture can be the dominant environmental parameter governing cadaver decomposition in soil. Forensic Sci Int 200:60–66

da Cruz GCF (2020) The urban area of the Verde River Basin and the environmental impacts caused by the urbanization of Ponta Grossa–PR–Brasil A área urbana da bacia do rio Verde e os impactos ambientais provocados pela urbanização de Ponta Grossa-PR–Brasil. Braz J Dev 6:87916–87934

de Oliveira JA, Cássaro FA, Pires LF (2021) Estimating soil porosity and pore size distribution changes due to wetting-drying cycles by morphometric image analysis. Soil Tillage Res 205:104814

Donagemma GK, Viana JM, de Almeida BG, et al (2017) Análise granulométrica.

Fu Y, Horton R, Heitman J (2021) Estimation of soil water retention curves from soil bulk electrical conductivity and water content measurements. Soil Tillage Res 209:104948

Grahn Y, Mendlowicz Mauller P, Breuer P, et al (2010) The Furnas/Ponta Grossa contact and the age of the lowermost Ponta Grossa Formation in the Apucarana Sub-basin (Paraná Basin, Brazil): integrated palynological age determination. Rev Bras Paleontol 13:89–102

Greenland DJ (1977) Soil damage by intensive arable cultivation: temporary or permanent? Philos Trans R Soc Lond B Biol Sci 281:193–208

Hammer Ø, Harper DA, Ryan PD (2001) PAST: Paleontological statistics software package for education and data analysis. Palaeontol Electron 4:9

Hegde P, Gaur N, Abney R, et al (2026) Effects of Tillage and Fertilization on Soil Structure in a Native Piedmont Grassland. Available SSRN 6947710

Hou X, Qi S, Liu F (2023) Soil water retention and pore characteristics of intact loess buried at different depths. Sustainability 15:14890

Jenner M (2005) Death, Decomposition and Dechristianisation? Public Health and Church Burial in Eighteenth-Century England. Engl Hist Rev 120:615–632. https://doi.org/10.1093/ehr/cei123

Junkins EN, Carter DO (2017) Relationships between Human Remains, Graves and the Depositional Environment. In: Schotsmans EMJ, Márquez-Grant N, Forbes SL (eds) Taphonomy of Human Remains: Forensic Analysis of the Dead and the Depositional Environment, 1st edn. Wiley, pp 143–154

Karahan G, Erşahin S (2017) Relating Macropore Flow to Soil Parametric and Morphological Variables. Soil Sci Soc Am J 81:1014–1024. https://doi.org/10.2136/sssaj2016.10.0327

Kong C, Camps-Arbestain M, Clothier B (2021) Influence of the physical properties of pumice and biochar amendments on the soil's mobile and immobile water: implications for use in saline environments. Soil Res 60:234–241

Krzeminska DM, Bogaard TA, Debieche T-H, et al (2014) Field investigation of preferential fissure flow paths with hydrochemical analysis of small-scale sprinkling experiments. Earth Surf Dyn 2:181–195

Lins E, Lins M, Lins C (2019) Negative environmental impacts generated by cemetery: Case study. Int J Adv Sci Res 4:16–19

Maia FC de O, Bufon VB, Leão TP (2018) Retention curves and available water capacity in latosols. Eng Agríc 38:546–552

Marini AF, Manhães AJP, Sales DDS, et al (2025) CEMETERIES AND ENVIRONMENTAL CONTAMINATION: STRATEGIES FOR CONTROL, MONITORING AND REMEDIATION. Rev Gest Soc E Ambient 19:1–14

Morandi L, De Borba WF, Da Ros CO, et al (2024) Soil contamination in a cemetery area: a case study in Nova Hartz City—RS, Brazil. Environ Sci Eur 36:95. https://doi.org/10.1186/s12302-024-00864-2

Mordhorst A, Zimmermann I, Fleige H, Horn R (2022) Environmental risk of (heavy) metal release from urns into cemetery soils. Sci Total Environ 817:152952. https://doi.org/10.1016/j.scitotenv.2022.152952

Neckel A, Costa C, Mario DN, et al (2017) Environmental damage and public health threat caused by cemeteries: a proposal of ideal cemeteries for the growing urban sprawl. Urbe Rev Bras Gest Urbana 9:216–230. https://doi.org/https://doi.org/10.1590/2175-3369.009.002.AO05

Ngolo AO, Oliveira FS de, Oliveira MF de, Fernandes RBA (2023) Microstructural changes in oxisols under long-term different management systems. Rev Bras Cienc Solo 47:e0230051

Orozco-López E, Muñoz-Carpena R, Gao B, Fox GA (2018) Riparian vadose zone preferential flow: Review of concepts, limitations, and perspectives. Vadose Zone J 17:1–20

Ottoni MV, Teixeira WG, Reis AMH dos, et al (2025) Saturated hydraulic conductivity and steady-state infiltration rate database for Brazilian soils. Rev Bras Ciênc Solo 49:e0240003. https://doi.org/https://doi.org/10.36783/18069657rbcs20240003

Pires LF, Roque WL, Rosa JA, Mooney SJ (2019) 3D analysis of the soil porous architecture under long term contrasting management systems by X-ray computed tomography. Soil Tillage Res 191:197–206

Ramesh T, Bolan NS, Kirkham MB, et al (2019) Soil organic carbon dynamics: Impact of land use changes and management practices: A review. Adv Agron 156:1–107

Reatto A, Bruand A, de Souza Martins E, et al (2009) Development and origin of the microgranular structure in Latosols of the Brazilian Central Plateau: Significance of texture, mineralogy, and biological activity. Catena 76:122–134

Schaefer CEGR, Siqueira RG, Pereira LF, et al (2025) Brazilian Latossolos (Ferralsols, Oxisols) from different biomes: a multiproxy study on the spatial variability of the most weathered tropical soils in South America. Geoderma Reg 43:e01012. https://doi.org/10.1016/j.geodrs.2025.e01012

Soil Survey Staff A (2014) Keys to soil taxonomy. Government Printing Office

575 Stepniewski W, Gliński J, Ball BC (1994) Effects of compaction on soil aeration properties. In:
576 Developments in agricultural engineering. Elsevier, pp 167–189

577 Teixeira PC, Donagemma GK, Fontana A, Teixeira WG (2017) Manual de métodos de análise de
578 solo

579 Tewari S, Virmani P, Saxena G, et al (2025) Microbe-Based Green Funeral Practices: Dying to
580 Go Green. J Biol Res Rev 1. https://doi.org/10.5455/JBRR.20240913095614

581 Van Genuchten MTh (1980) A Closed-form Equation for Predicting the Hydraulic Conductivity
582 of Unsaturated Soils. Soil Sci Soc Am J 44:892–898.
583 https://doi.org/10.2136/sssaj1980.03615995004400050002x

584 Zhang X (2023) Soil Mineral Particle Size Analysis: Validation of Stokes' Law

585 Żychowski J, Bryndal T (2015) Impact of cemeteries on groundwater contamination by bacteria
586 and viruses–a review. J Water Health 13:285–301

587